Electronic Supplementary Material (ESI) for Journal of Materials Chemistry A.

Supporting Information

Tailoring the cationic and anionic sites of $LaFeO_3$-based perovskite generates multiple vacancies for efficient water oxidation

Paul Blessington Selvadurai A.,[a,d,#] Tuzhi Xiong,[a,d,#] Peng Huang,[a,d] Qirong Tan,[a,d] Yongchao Huang[b], Hao Yang[c], M.-Sadeeq (Jie Tang) Balogun,*[,a,d]

[a]College of Materials Science and Engineering, Hunan University, Changsha 410082, China. E-mail: balogun@hnu.edu.cn

[b]Institute of Environmental Research at Greater Bay, Key Laboratory for Water Quality and Conservation of the Pearl River Delta, Ministry of Education, Guangzhou University, Guangzhou 510006, China.

[c]School of Chemistry & Chemical Engineering, Guangxi University, Nanning, 530004, China.

[d]Hunan Joint International Laboratory of Advanced Materials and Technology for Clean Energy, Hunan University, Changsha 410082, China.

Experimental Section Continues…

Synthesis of LFCMO

The synthesis of LFCMO was the same with that of H-LFCMO without the reduction process.

Synthesis of LFCO

The synthesis of LFCO was the same with that of LFCMO without the presence of $(NH_4)_6Mo_7O_{24}$.

Synthesis of LFO

The synthesis of LFO was the same with that of LFCO without the presence of $Cr(NO_3)_3.9H_2O$.

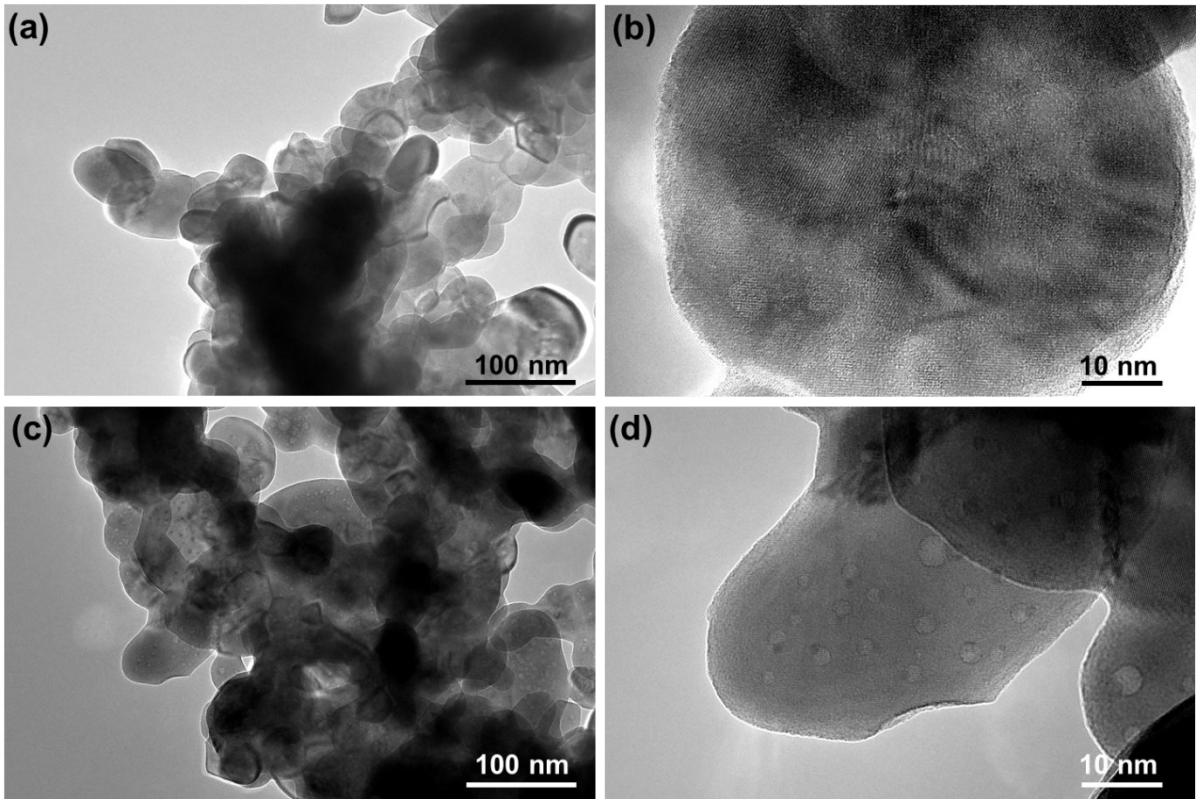

Figure S1. (a and b) Enlarge TEM images of LFCMO sample from Figure 1g. (c and d) Enlarged TEM images of H-LFCMO samples from Figure 1h.

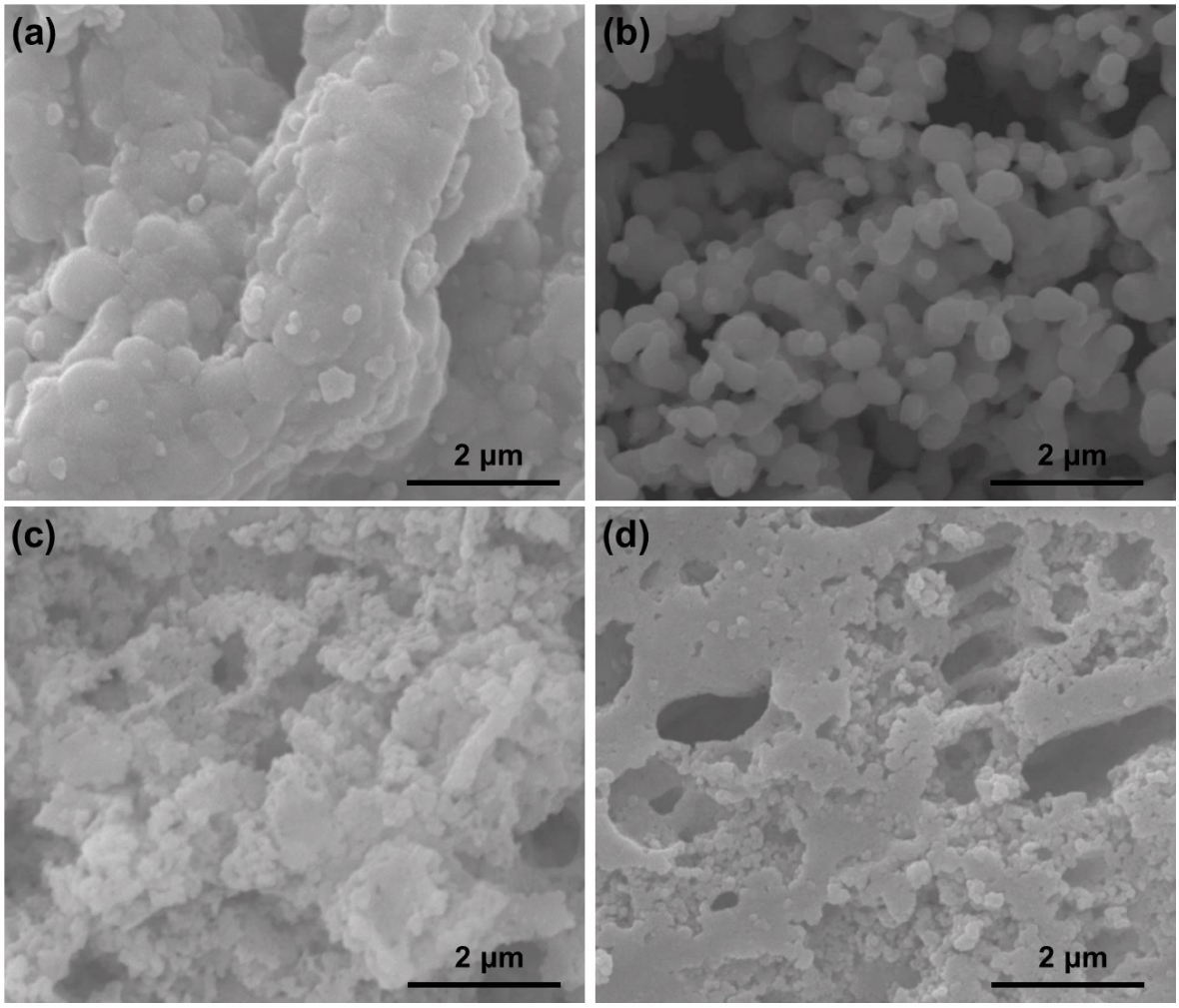

Figure S2. SEM images of (a) LFO, (b) LFCO, (c) LFCMO and (d) H-LFCMO samples.

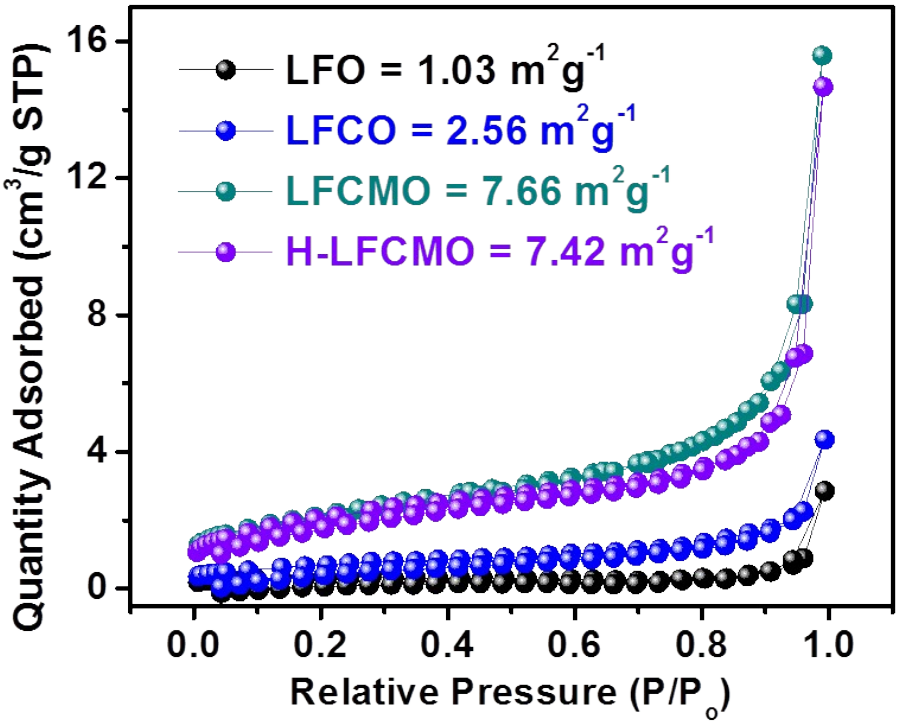

Figure S3. Nitrogen adsorption isotherms of the LFO, LFCO, LFCMO and H-LFCMO samples.

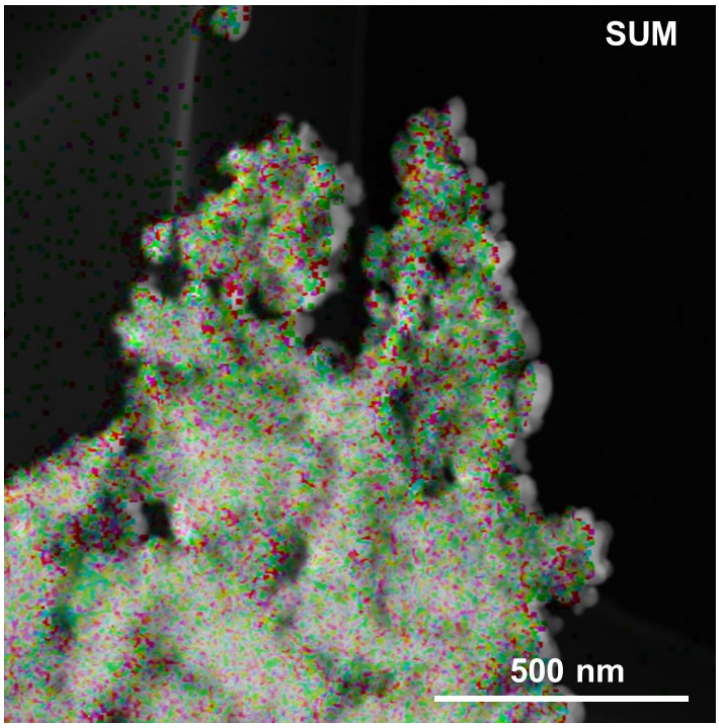

Figure S4. Corresponding EDX sum of the H-LFCMO sample.

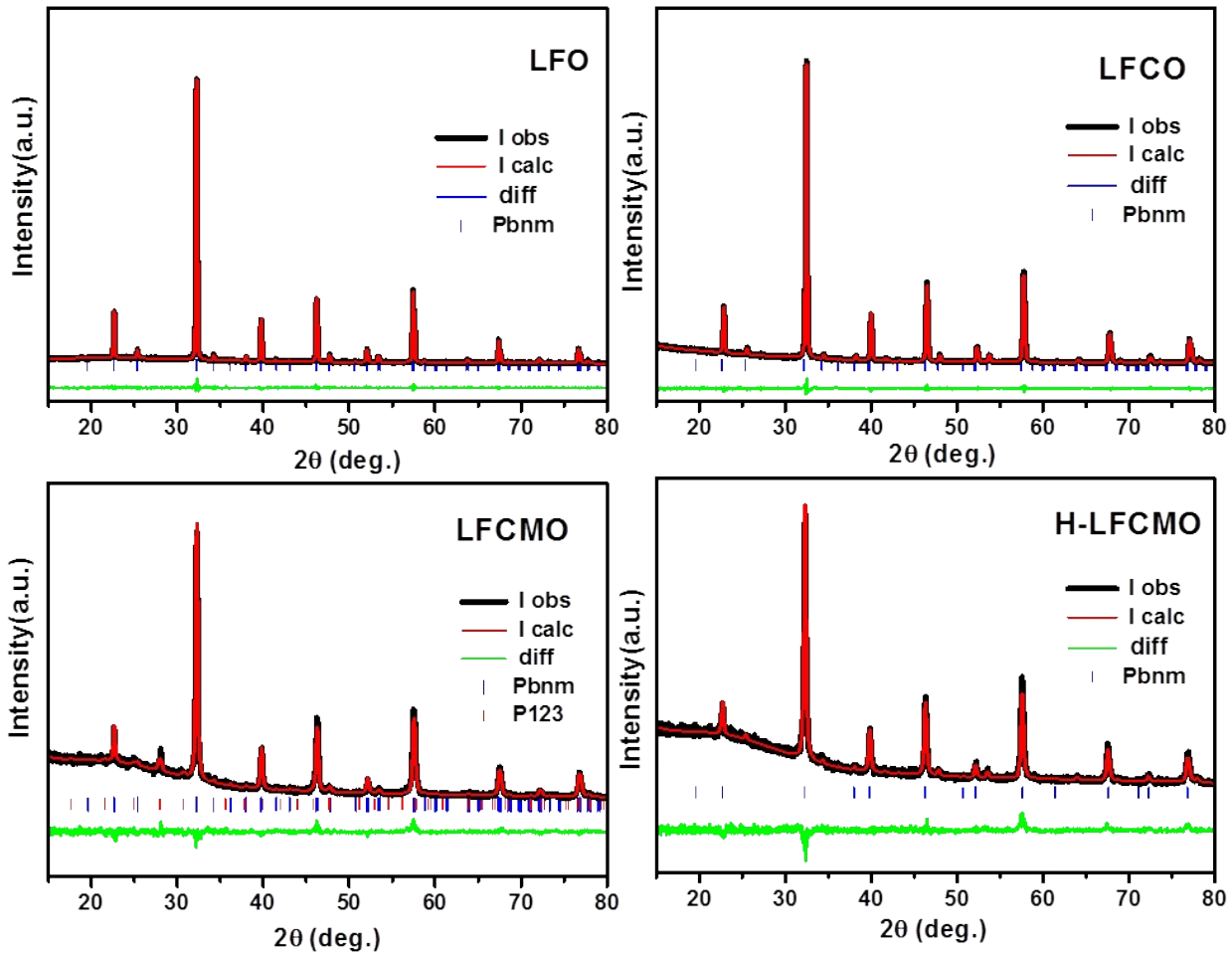

Figure S5. Reitveld refinement XRD patterns of the samples.

Table S1. The structural parameters derived from the refinement.

Samples	a (Å)	b (Å)	c (Å)	V (Å^3)	R_p	% R_{wp}	χ2
LF	5.559(2)	5.565(2)	7.857(4)	243.063	5.96	5.26	1.33
LFC25	5.549(4)	5.538(3)	7.836(5)	240.803	4.60	4.67	1.28
LFCM10	5.557(1)	5.553(1)	7.846(1)	242.112	6.79	7.52	1.52
H-LFCM10	5.555(1)	5.557(1)	7.848(2)	241.068	6.36	9.92	1.34

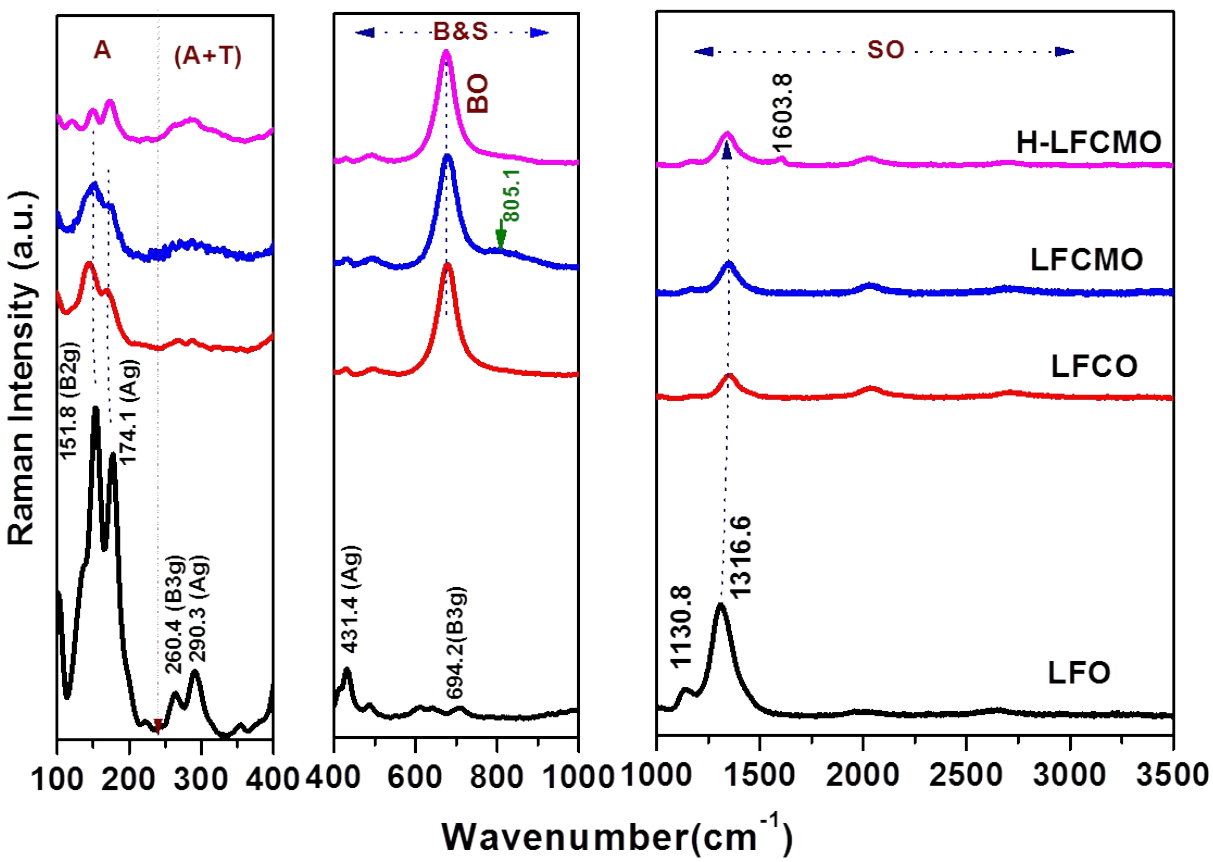

Figure S6. Raman spectra of the samples.

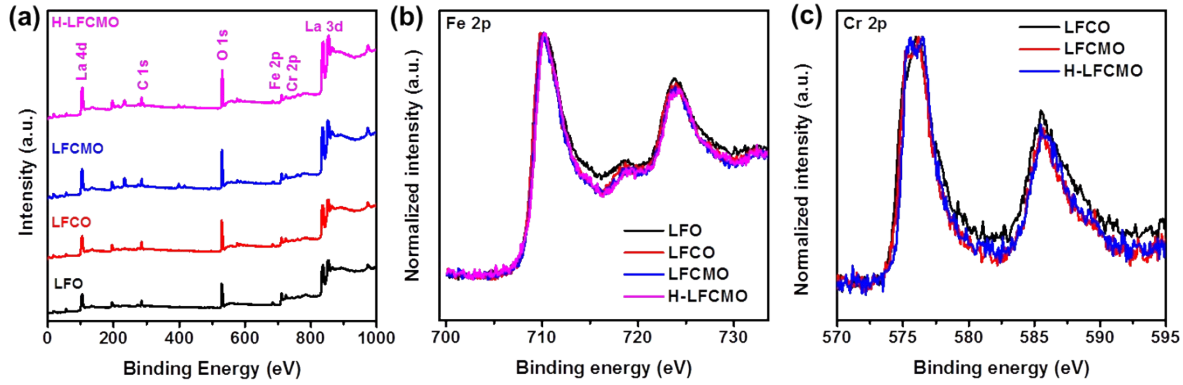

Figure S7. (a) Survey and (b) Fe 2p XPS spectra of the entire samples. (c) Cr 2p XPS spectra of LFCO, LFCMO and H-LFCMO.

Table S2. Comparisons of OER catalytic performances of H-LFCMO and other related ABO_3-based perovskites.

Catalysts	Substrate	Tafel ($mV\ dec^{-1}$)	η@10 mA cm^{-2}	Ref.
H-LFCMO	Nickel foam	97	263	This work
$Ba_{0.9}Sr_{0.1}C_{0.8}Fe_{0.1}Ir_{0.1}O_{3-\delta}$	Glassy Carbon	61.2	300	[1]
$La_{0.7}Sr_{0.3}MnO_3$	FTO	103	430	[2]
VG-$LaCoO_3$	Nickel foam	45	342	[3]
F-$Ba_{0.5}Sr_{0.5}C_{0.8}Fe_{0.2}O_{3-d}$	Glassy Carbon	102.65	220	[4]
$Sr(Co_{0.8}Fe_{0.2})_{0.7}B_{0.3}O_{3-\delta}$	Glassy Carbon	60	240	[5]
$SrCo_{0.4}Fe_{0.2}W_{0.4}O_{3-\delta}$	Glassy Carbon	58	292	[6]
CQDs@$Ba_{0.5}Sr_{0.5}C_{0.8}Fe_{0.2}O_{3-d}$	Nickel foam	66	350	[7]
a-$LaNiFeO_3$(t-d)	Nickel foam	36	189	[8]
$LaFeO_{2.85}Cl_{0.15}$	Glassy Carbon	67	500	[9]
LF-$_{0.25}$Ce	Glassy Carbon	71.5	330	[10]
$LaFe_{0.5}Mn_{0.5}O_3$	Glassy Carbon	108	454	[11]
$La_{0.9}Fe_{0.92}Ru_{0.08}O_{3-\delta}$-H-O	Glassy Carbon	39	380	[12]
$La_{0.4}Sr_{0.6}Ni_{0.5}Fe_{0.5}O_3$	Glassy Carbon	52.77	320	[13]
3DOM-LFC82	Glassy Carbon	56	410	[14]
$La_{0.2}Sr_{0.8}FeO_3$	Glassy Carbon	58	318	[15]
MoS_2-$SrCoO_{3-\delta}$	Glassy Carbon	38	351	[16]
$Ce_{0.8}Sr_{0.2}Co_{0.8}Fe_{0.2}O_{3-\delta}$	Glassy Carbon	40.7	440	[17]
80nm $LaCoO_3$	Glassy Carbon	69	490	[18]
$LaFe_{0.2}Ni_{0.8}O_3$	Glassy Carbon	50	302	[19]
$La_{1-x}Sr_xCo_{1-y}Fe_yO_{3-\delta}$	Carbon Fiber Paper	109	440	[20]

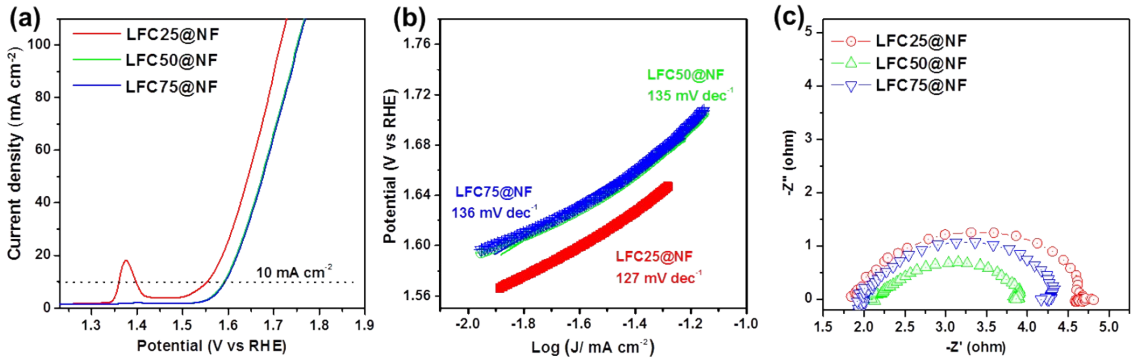

Figure S8. (a) LSV curves, (b) Tafel slope and (c) EIS spectra LFCO with different Cr content.

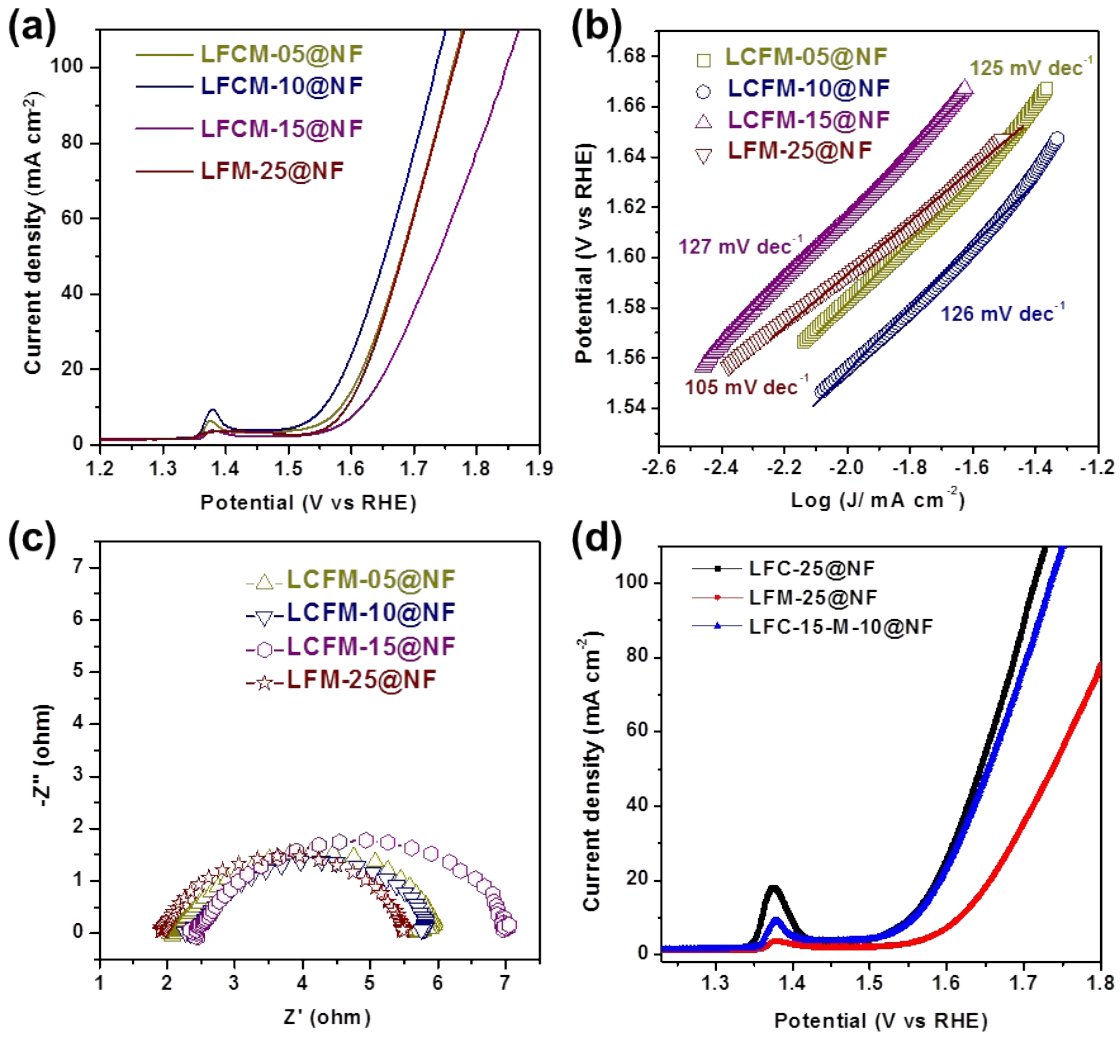

Figure S9. (a) LSV curves, (b) Tafel slope and (c) EIS spectra LFCMO with different Mo content. (d) LSV curves of LFCO-25 and LFMO-25.

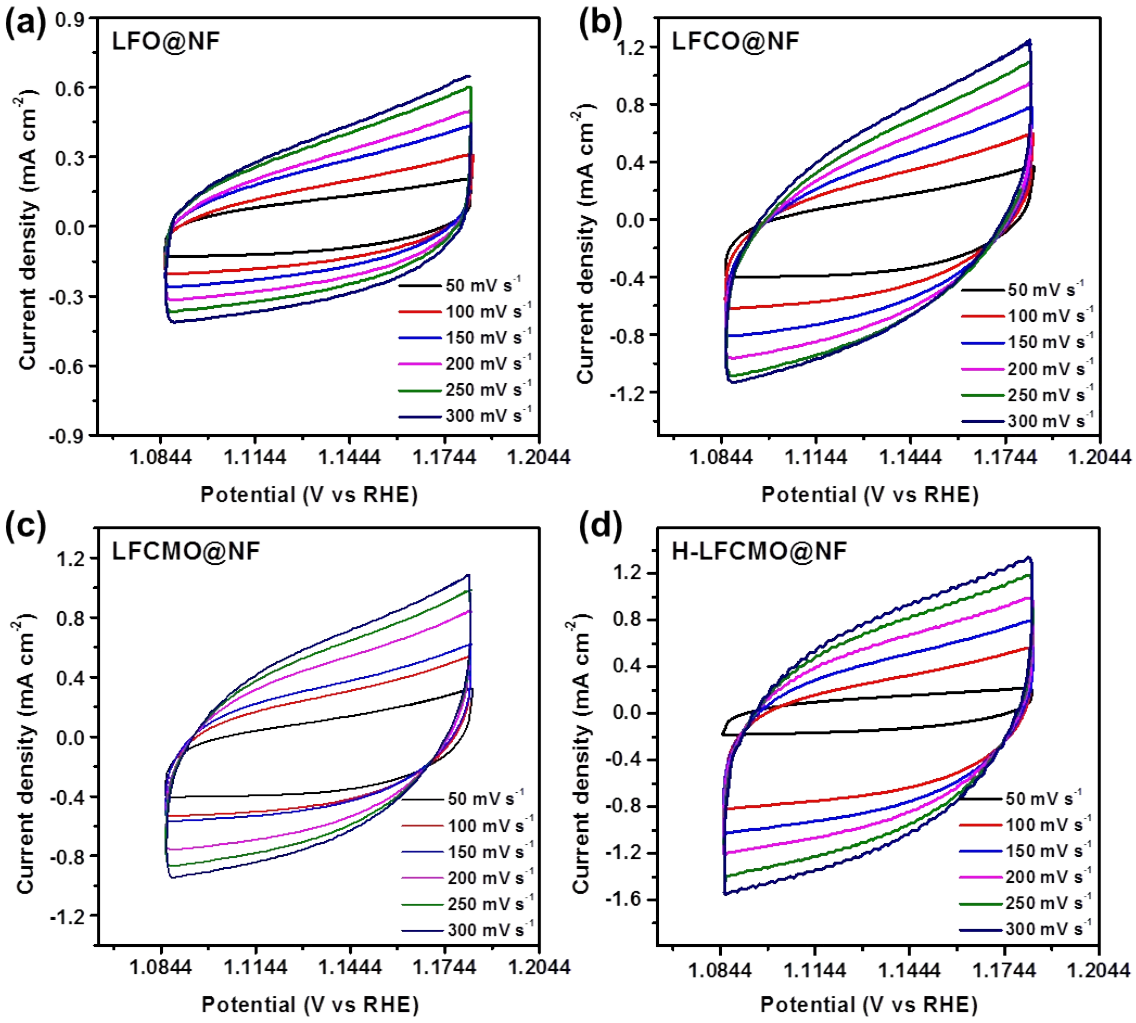

Figure S10. CV curves of (a) LFO, (b) LFCO, (c) LFCMO and (c) H-LFCMO at different scan rates ranging from 50 – 300 mV s^{-1}.

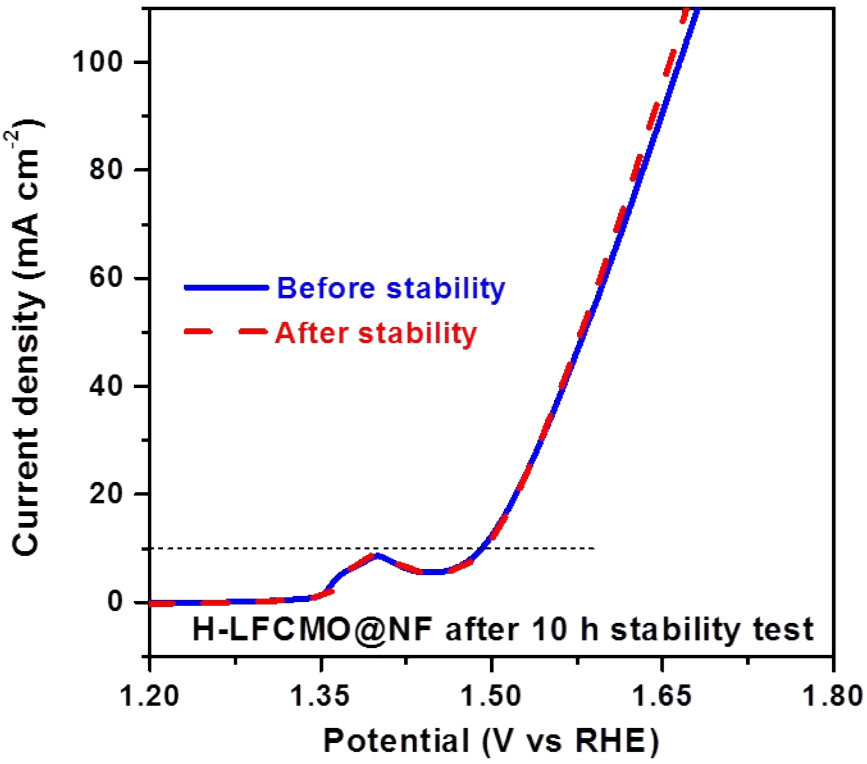

Figure S11. LSV curves of H-LFCMO before and after stability test.

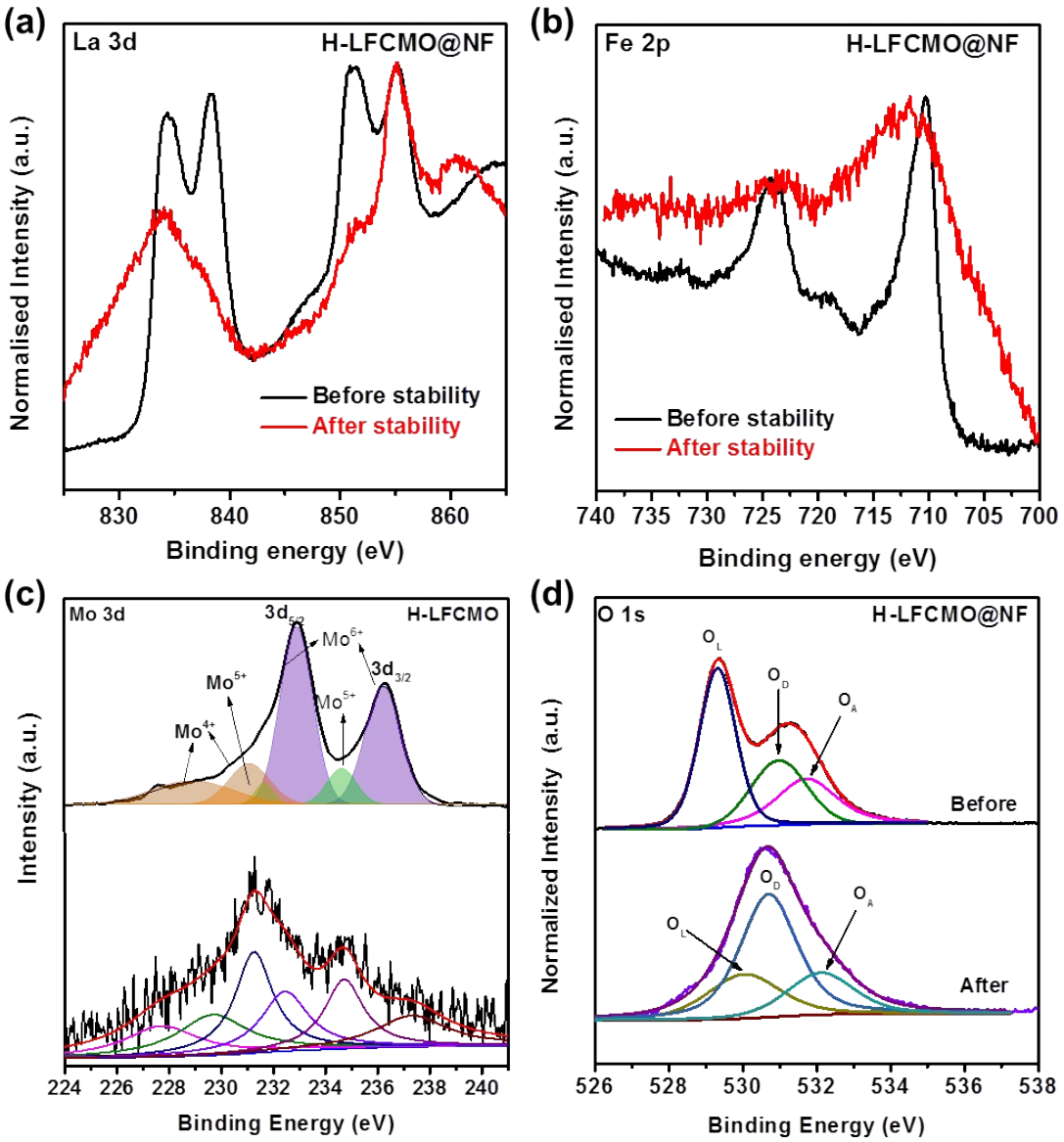

Figure S12. (a) La 3d, (b) Fe 2p, (c) Mo 3d and (d) O 1s XPS spectra of H-LFCMO before and after stability test.

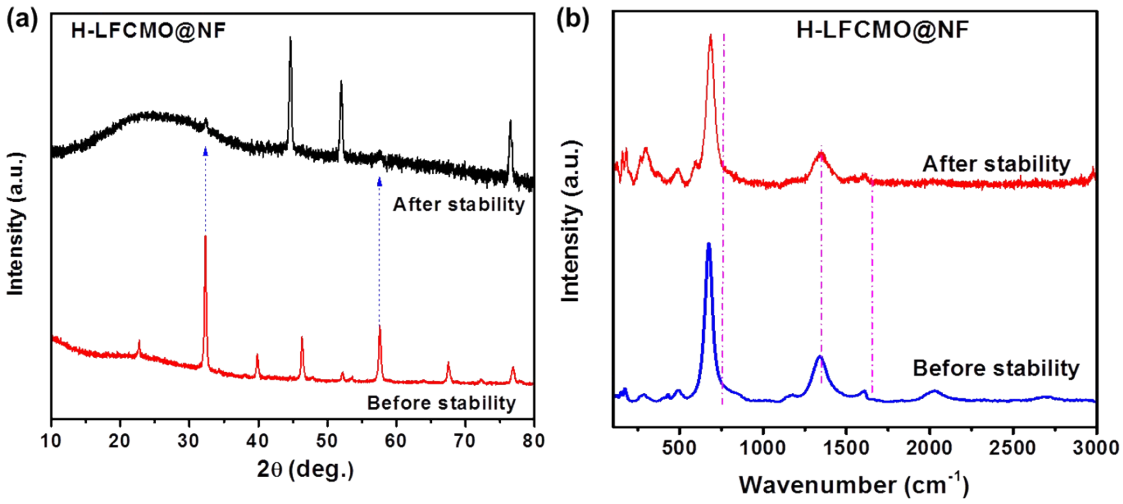

Figure S13. (a) XRD and (b) Raman spectra of H-LFCMO before and after stability test.

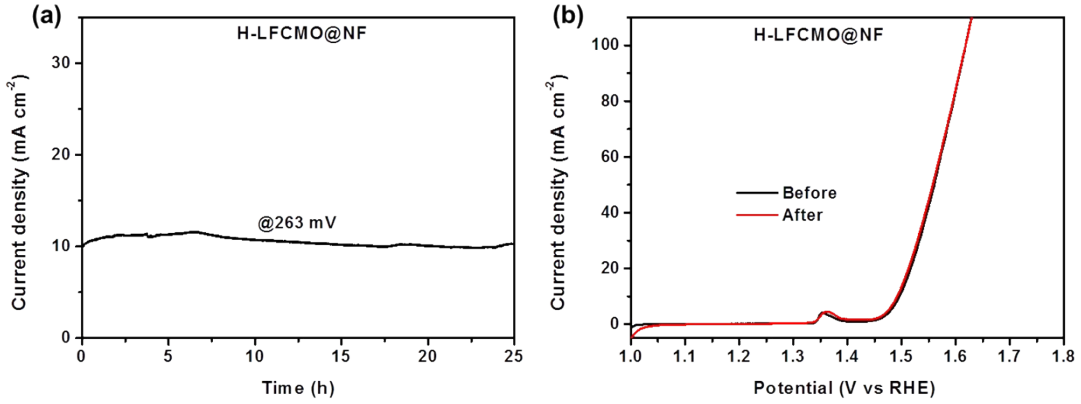

Figure S14. (a) Chronopotentiometry stability test of H-LFCMO@NF catalyst. (b) LSV curves of H-LFCMO@NF catalyst before and after stability test.

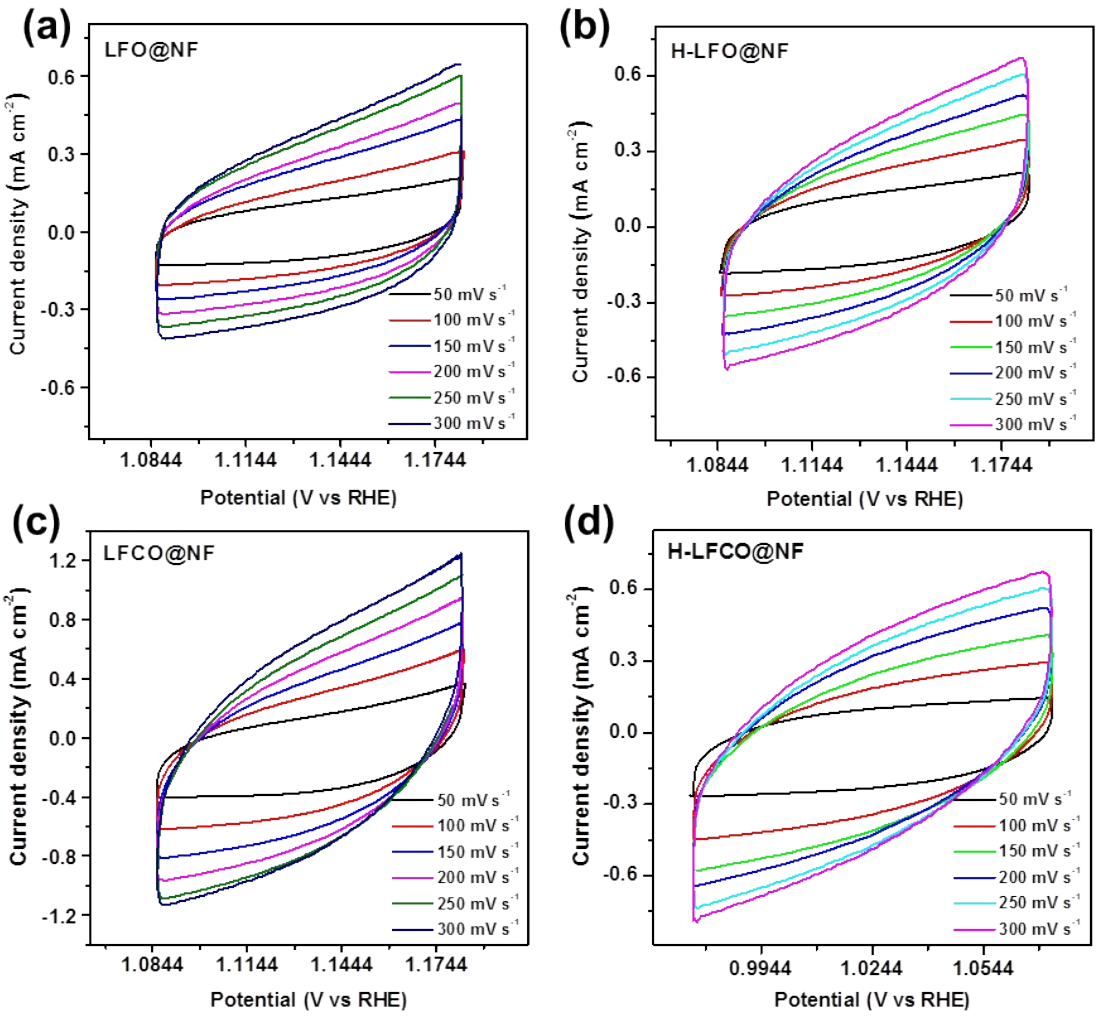

Figure S15. CV curves of (a) LFO, (b) H-LFO, (c) LFCO and (c) H-LFCO at different scan rates ranging from 50 – 300 mV s^{-1}.

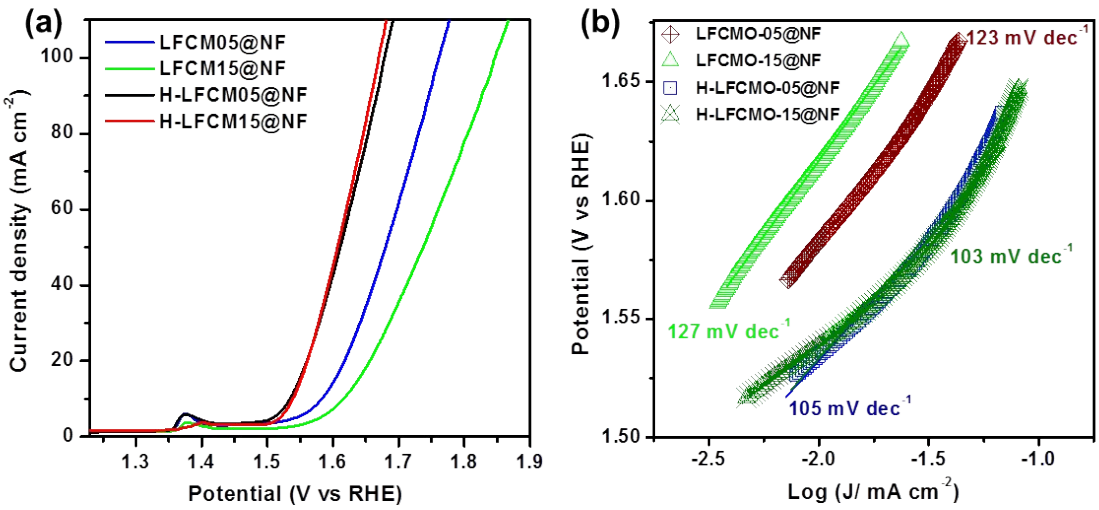

Figure S16. (a) LSV curves and (b) Tafel slopes of LFCMO with different Mo content and their corresponding hydrogenated catalysts.

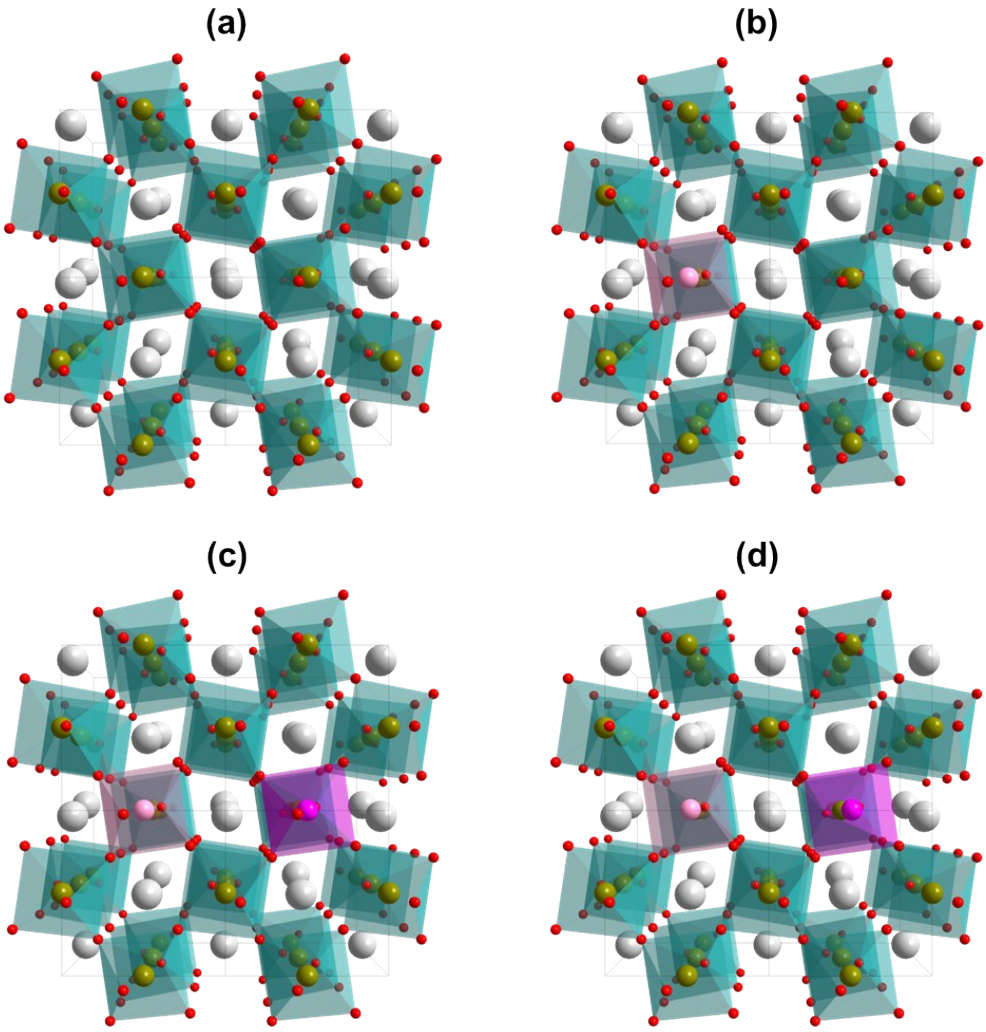

Figure S17. Optimized structure of (a) LFO (b) LFCO (c) LFCMO and (d) H-LFCMO. Ash, deep green, light green, pink and red balls represents La, Fe, Cr, Mo and O atoms, respectively.

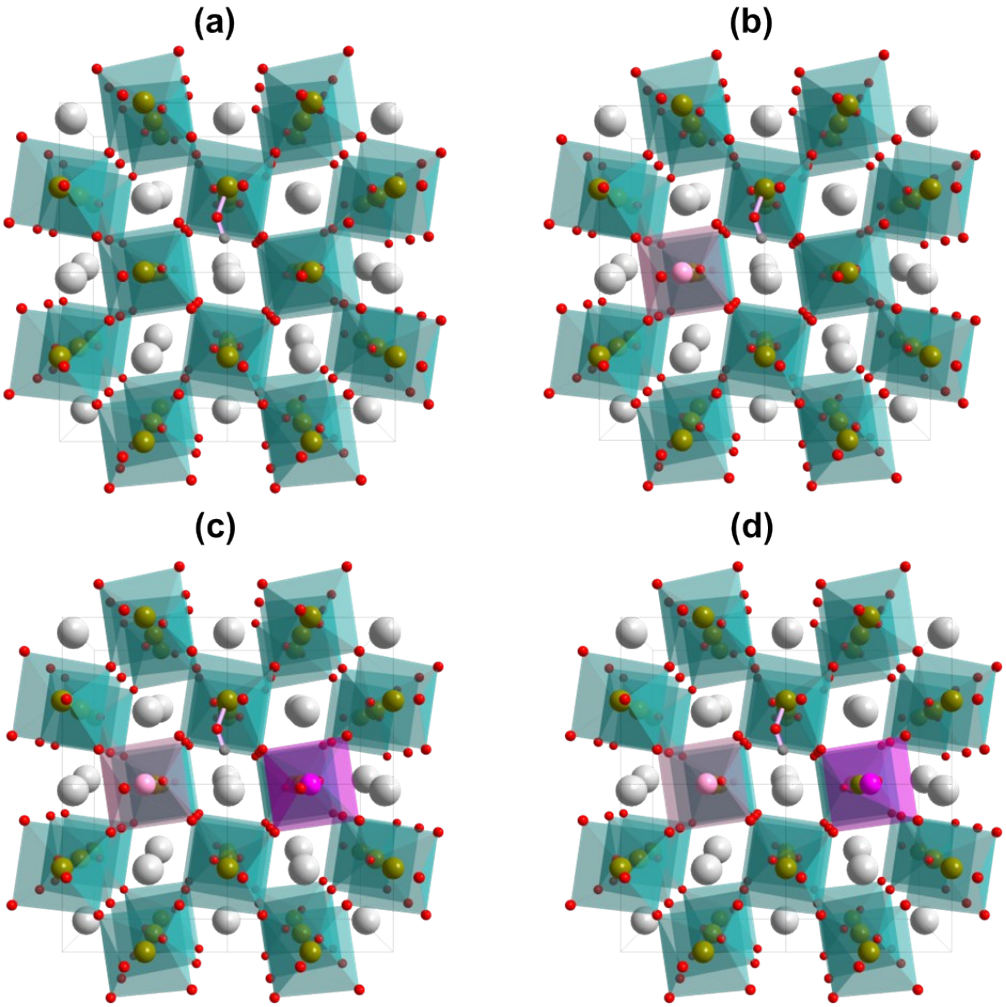

Figure S18. Optimized structure of (a) LFO-OH, (b) LFCO-OH, (c) LFCMO-OH and (d) H-LFCMO-OH. Ash, deep green, light green, pink and red balls represents La, Fe, Cr, Mo and O atoms, respectively.

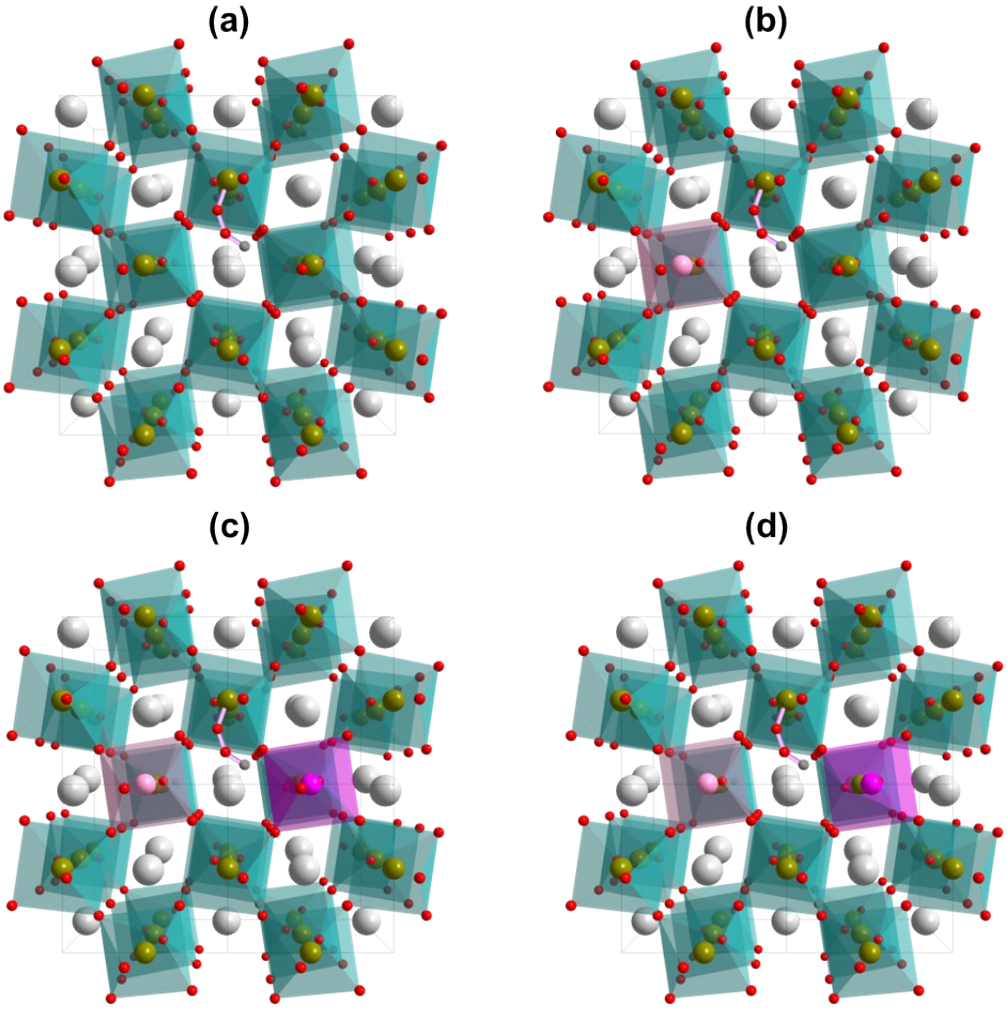

Figure S19. Optimized structure of (a) LFO-OOH, (b) LFCO-OOH, (c) LFCMO-OOH and (d) H-LFCMO-OOH. Ash, deep green, light green, pink and red balls represents La, Fe, Cr, Mo and O atoms, respectively.

The binding energy and the absorption energy with refer to the gaseous state of H_2O and H_2 molecules were calculated based on Wang et al. analysis. [21] The obtained results are tabulated in Table S2 below.

Table S3. Calculated binding energy and absorption energy with refer to the gaseous state of H_2O and H_2 molecules in the units of eV.

Structures	**Binding Energy**		**Absorption Energy**	
	OH	**OOH**	**OH**	**OOH**
$LaFeO_3$	-2.073	-1.068	1.051	4.626
$LaFe_{0.9}Cr_{0.1}O_3$	-3.425	-1.695	0.733	3.806
$LaFe0.8Cr_{0.1}Mo_{0.1}O_3$	-1.050	-1.923	1.752	4.896

The calculated values for FeO_2 terminated $LaFeO_3$ surface is in consistent with the previous reported results. [21, 22] Among all $LaFe0.8Cr_{0.1}Mo_{0.1}O_3$ shows high absorption characteristics compared to the other configurations considered. The Gibbs free energy of formation from elements of FeO_2 terminated $LaFeO_3$ surface, $LaFe_{0.9}Cr_{0.1}O_3$ surface, $LaFe0.8Cr_{0.1}Mo_{0.1}O_3$ surface with OH* and OOH* species are given in Table S3. The computed Gibbs free energy of formation from the elements of $LaFeO_3$ surface is in consistent with the experimental result. [23]

Table S4. Calculated Gibbs free energy of formation in the units of eV.

Structures	**Free Energy**		
	LFO	LFCO	LFCMO
Surface	-11.0323	-13.7176	-15.5906
Surface + OH*	-13.2235	-15.7752	-16.3506
Surface + OOH*	-15.2205	-17.2161	-18.7168

References:

[1] Q. Luo, D. Lin, W. Zhan, W. Zhang, L. Tang, J. Luo, Z. Gao, P. Jiang, M. Wang, L. Hao, K. Tang, *ACS Appl. Energy Mater.* **2020**, 3, 7149.

[2] S. Bhowmick, A. Dhankhar, T. K. Sahu, R. Jena, D. Gogoi, N. R. Peela, S. Ardo, M. Qureshi, *ACS Appl. Energy Mater.* **2020**, 3, 1279.

[3] T. Zhao, Y. Wang, X. Chen, Y. Li, Z. Su, C. Zhao, *ACS Sustain. Chem. Eng.* **2020**, 8, 4863.

[4] J. Xiong, H. Zhong, J. Li, X. Zhang, J. Shi, W. Cai, K. Qu, C. Zhu, Z. Yang, S. P. Beckman, H. Cheng, *Appl. Catal. B-Environ.* **2019**, 256, 117817.

[5] S. She, Y. Zhu, Y. Chen, Q. Lu, W. Zhou, Z. Shao, *Adv. Energy Mater.* **2019**, 9, 1900429.

[6] G. Chen, Z. Hu, Y. Zhu, Z.-G. Chen, Y. Zhong, H.-J. Lin, C.-T. Chen, L. H. Tjeng, W. Zhou, Z. Shao, *J. Mater. Chem. A* **2018**, 6, 9854.

[7] G. Li, S. Hou, L. Gui, F. Feng, D. Zhang, B. He, L. Zhao, *Appl. Catal. B-Environ.* **2019**, 257, 117919.

[8] G. Chen, Y. Zhu, H. M. Chen, Z. Hu, S.-F. Hung, N. Ma, J. Dai, H.-J. Lin, C.-T. Chen, W. Zhou, Z. Shao, *Adv. Mater.* **2019**, 31, 1900883.

[9] J. Zhang, Y. Cui, L. Jia, B. He, K. Zhang, L. Zhao, *Int. J. Hydrogen. Energ.* **2019**, 44, 24077.

[10] Y. Dai, J. Yu, Z. Zhang, C. Cheng, P. Tan, Z. Shao, M. Ni, *ACS Appl. Mater. Interfaces* **2021**, 13, 2799.

[11] J. Zhang, S. Zhu, Y. Min, Q. Xu, *Front. Mater. Sci.* **2020**, 14, 459.

[12] L. Fu, J. Zhou, L. Zhou, J. Yang, Z. Liu, K. Wu, H. Zhao, J. Wang, K. Wu, *Chem. Eng. J.* **2021**, 418, 129422.

[13] Q. Guo, X. Li, H. Wei, Y. Liu, L. Li, X. Yang, X. Zhang, H. Liu, Z. Lu, *Front. Chem.* **2019**, 7.

[14] J. Dai, Y. Zhu, Y. Zhong, J. Miao, B. Lin, W. Zhou, Z. Shao, *Adv. Mater. Interfaces* **2019**, 6, 1801317.

[15] Z. Shen, Y. Zhuang, W. Li, X. Huang, F. E. Oropeza, E. J. M. Hensen, J. P. Hofmann, M. Cui, A. Tadich, D. Qi, J. Cheng, J. Li, K. H. L. Zhang, *J. Mater. Chem. A* **2020**, 8, 4407.

[16] A. Curcio, J. Wang, Z. Wang, Z. Zhang, A. Belotti, S. Pepe, M. B. Effat, Z. Shao, J. Lim, F. Ciucci, *Adv. Funct. Mater.* **2021**, 31, 2008077.

[17] C. B. Njoku, B. P. Doyle, E. Carleschi, R. J. Kriek, *Electroanal.* **2020**, 32, 3131.

[18] S. Zhou, X. Miao, X. Zhao, C. Ma, Y. Qiu, Z. Hu, J. Zhao, L. Shi, J. Zeng, *Nat. Commun.* **2016**, 7, 11510.

[19] H. Wang, J. Wang, Y. Pi, Q. Shao, Y. Tan, X. Huang, *Angew. Chem. Int. Ed.* **2019**, 58, 2316.

[20] R. Majee, S. Chakraborty, H. G. Salunke, S. Bhattacharyya, *ACS Appl. Energy Mater.* **2018**, 1, 3342.

[21] Y. Wang, H.-P. Cheng, *J. Phys. Chem. C* **2013**, 117, 2106.

[22] I. C. Man, H.-Y. Su, F. Calle-Vallejo, H. A. Hansen, J. I. Martínez, N. G. Inoglu, J. Kitchin, T. F. Jaramillo, J. K. Nørskov, J. Rossmeisl, *ChemCatChem* **2011**, 3, 1159.

[23] J. Cheng, A. Navrotsky, X.-D. Zhou, H. U. Anderson, *J. Mater. Res.* **2005**, 20, 191.